

1 **Effect of water vapour on the determination of Aerosol Direct Radiative Effect based on the**
2 **AERONET fluxes**

3 **J. Huttunen¹, A. Arola¹, G. Myhre², A.V. Lindfors¹, T. Mielonen¹, S. Mikkonen³, J. Schafer⁴, S. N.**
4 **Tripathi⁵, M. Wild⁶, M. Komppula¹ and K. E. J. Lehtinen^{1,3}**

5 [1]{Finnish Meteorological Institute (FMI), Kuopio Unit, Finland.}

6 [2]{Center for International Climate and Environmental Research - Oslo, Norway.}

7 [3]{Department of Applied Physics, University of Eastern Finland, Kuopio, Finland.}

8 [4]{NASA/Goddard Space Flight Center (GSFC), Biospheric Sciences Branch, Greenbelt, MD, USA.}

9 [5]{Department of Civil Engineering, Indian Institute of Technology, Kanpur, India.}

10 [6]{Institute for Atmospheric and Climate Science, ETH Zurich, Switzerland.}

11 Corresponding author: J. Huttunen, Finnish Meteorological Institute, Kuopio Unit, P.O. Box
12 1627, FI-70211 Kuopio, Finland. (jani.huttunen@fmi.fi)

13

14 **Abstract**

15 The Aerosol Direct Radiative Effect (ADRE) is defined as the change in the solar radiation flux, F , due
16 to aerosol scattering and absorption. The difficulty in determining ADRE stems mainly from the need
17 to estimate F without aerosols, F^0 , with either radiative transfer modelling and knowledge of the
18 atmospheric state, or regression analysis of radiation data down to zero aerosol optical depth (AOD), if
19 only F and AOD are observed. This paper examines the regression analysis method by using modeled
20 surface data products provided by the AEROSOL ROBOTIC NETWORK (AERONET). We extrapolated F^0 by
21 two functions: a straight linear line and an exponential nonlinear decay. The exponential decay
22 regression is expected to give a better estimation of ADRE with a few percents larger extrapolated F^0
23 than the linear regression. We found that, contrary to the expectation, in most cases the linear

24 regression gives better results than the nonlinear. In such cases the extrapolated F^0 represents an
25 unrealistically low [water vapour column \(WVC\)](#), resulting in underestimation of attenuation caused by
26 the water vapour, and hence too large F^0 and overestimation of the magnitude of ADRE. The nonlinear
27 ADRE is generally 40-50 % larger in magnitude than the linear ADRE due to the extrapolated F^0
28 difference. Since for a majority of locations, AOD and [water vapour column \(WVC\)](#) have a positive
29 correlation, the extrapolated F^0 with the nonlinear regression fit represents an unrealistically low WVC,
30 and hence too large F^0 . The systematic underestimation of F^0 with the linear regression is compensated
31 by the positive correlation between AOD and water vapour, providing the better result.

32

33 **1. Introduction**

34 Significant uncertainties exist in the current estimates of aerosol effects on climate (IPCC, 2013). This
35 holds also for the aerosol direct radiative effect (ADRE) and aerosol direct radiative forcing (ADRF).
36 The ADRE defines the attenuation of the (cloud free sky) surface solar radiation flux (F) due to aerosol
37 scattering and absorption. Herein, we consider the solar radiation flux at the surface, although ADRE
38 applies also for the longwave flux and above the atmosphere. In the definitions of ADRE and ADRF,
39 effects relate to both anthropogenic and natural aerosol particles, while forcing refers to the impact of
40 anthropogenic aerosol particles. Although, e.g., Myhre (2009) recently showed an increment of the
41 consistency between observation based and global aerosol model estimates, with a reduction in the
42 uncertainty of this effect, other studies (e.g., Loeb and Su, 2010) highlight that considerable
43 uncertainties are still associated with ADRE, mainly due to the uncertainties in single scattering albedo
44 (SSA). Satheesh and Ramanathan (2000) employed a method in which ADRE is estimated using the
45 aerosol direct effect efficiency (ADREE), which is the ADRE normalized by the aerosol optical depth
46 (AOD), and it is estimated by fitting a straight line into surface solar flux and AOD observations. A

47 linear dependence between aerosol attenuation and AOD has been commonly assumed when estimating
48 ADRE (e.g., Kaufman et al., 2002; Bush and Valero, 2002, 2003; Dumka et al., 2006; Roger et al.,
49 2006; di Sarra et al., 2008; Garcia et al., 2009; Satheesh et al., 2010). Typical attenuation of radiation
50 intensity, however, implies nonlinear decay, as considered by e.g. Conant et al. (2003), Markowicz et
51 al. (2008) and Kudo et al. (2010). Thus, a linear fit to F and AOD data may result in an incorrect
52 extrapolation of F^0 .

53 The aim of this paper is to examine the uncertainties involved in estimating ADRE, both using
54 the linear fitting method and a nonlinear approach if F and AOD data are available from surface or
55 satellite measurements. For this, we use Aerosol Robotic Network (AERONET) products
56 (<http://aeronet.gsfc.nasa.gov/>) from all available AERONET stations, which cover different aerosol
57 types and surface reflectance properties and provide modelled surface solar radiation fluxes also. We
58 conducted our analysis using these modeled fluxes since they represent realistically enough the aerosol-
59 induced relative changes in F and furthermore give an estimate for F^0 , which is self-consistent within
60 the selected F (AOD) data set. As AERONET provides an estimation of F^0 , we can compare the
61 estimations immediately with the baseline (AERONET). Special attention is paid to the possible effect
62 of water vapour on estimating ADRE.

63

64 **2. Methods and data**

65 [AERONET is a ground-based remote-sensing global network of Cimel sun photometers \(Holben et al.,](#)
66 [1998\) including the AERONET inversion code with radiative transfer code implementation. The](#)
67 [inversion strategy, described in Dubovik and King \(2000\), provides a group of parameters, e.g. AOD,](#)
68 [Ångström exponent \(AE\) and water vapour column \(WVC\) from the sun measurements and e.g. SSA,](#)

69 asymmetry parameter (ASYM) and size distribution from the sky measurements. AOD is provided with
70 wavelength channels 340, 380, 440, 500, 670, 870, 1020 and 1640 nm (all or some of these, depending
71 on site of AERONET), WVC from 940 nm and e.g. SSA and ASYM from 440, 670, 870 and 1020 nm.
72 The Discrete Ordinates (DISORT) provides broadband fluxes (both at the top of atmosphere and at the
73 surface, with and without aerosols), calculated with the correlated-k distribution in the Global
74 Atmospheric Model (GAME) code from 200 nm to 4000 nm. The ozone is based on monthly averaged
75 climatology by the Total Ozone Mapping Spectrometer (TOMS). Moreover, the US standard 1976
76 atmosphere model sets the atmospheric gaseous profile. The surface reflectivity is approximated by the
77 Bidirectional Reflectance Distribution Function (BRDF) and observations from the Moderate-
78 Resolution Imaging Spectroradiometer (MODIS). More details about the AERONET description from
79 e.g. García et al. (2012). The uncertainty of AOD is 0.01-0.02 depending on the wavelength (Eck et al.,
80 1999), the uncertainty in SSA is approximately 0.03 (Dubovik et al., 2000), and the uncertainty in
81 WVC of 12 % (Holben et al., 1998). AERONET is a ground-based remote-sensing global network of
82 Cimel sun photometers (Holben et al., 1998), retrieving e.g. spectral AOD, SSA and water vapor
83 column (WVC) (Dubovik et al., 2000). In addition to the retrieved aerosol properties, AERONET
84 inversion product provides also modeled radiative fluxes (both at top of atmosphere and at surface) that
85 are based on the AERONET measurements. We used broad-band modeled surface shortwaveSW fluxes
86 from this data set. In this study, level 1.5 sky AERONET data are divided into groups by station, season
87 (December-February, March-May, June-August and September-November) and by solar zenith angle
88 (SZA) (3° steps in the range 0°-80°). A dataset was included in the analysis if it had at least 20
89 observations and the data contained AOD 550 nm values above 0.3 and below 0.1. We chose to use
90 level 1.5 data because using level 2.0 would leave out all quality-assured data with AOD 440 nm < 0.4
91 (including e.g. quality assured SSA and *F* calculations). The drawback of this choice is that at these low
92 values of AOD, there are significant uncertainties in the optical properties retrieved. This is especially

93 true for SSA, which is an important parameter. Thus, we applied all other level 2 criteria except for
94 AOD (and SZA) limit, in order to enhance the accuracy of the data set selected. Moreover, we have
95 imposed an additional data flagging criterion, removing those SSA points at the AOD 440 nm < 0.4,
96 which are outside the average SSA \pm standard deviation, defined for the AOD 440 nm > 0.4.

97 ADRE at the surface is the difference between the solar flux with and without aerosols: ADRE
98 = $\Delta F = F^{aer} - F^0$ (F^{aer} is flux with aerosols). The major challenge obviously is the determination of F^0 .
99 The methodology for its estimation employed in this study is illustrated in Fig. 1, in which F^{aer}
100 (+symbols) is plotted as a function of AOD (from now on 550 nm) for the AERONET site in Kanpur
101 station (26° N, 80° E) for the spring months March-May with SZA = 69° \pm 1.5° (F^{aer} values were
102 normalized for the average earth-sun distance and cosine correction of $F^{aer} \cos \theta_{SZA}$ was done within SZA
103 ranges to its midpoints). F^0 represents the case AOD = 0, but with measurements only at AOD above
104 ca. 0.15, we have to extrapolate down to 0. In Fig. 1 we show two such extrapolations: a linear fit
105 (dashed line) and an nonlinear decay fit (solid line) with the data.

106 We chose this data subset since it represent a case in which the F^{aer} and AOD data exhibit the
107 natural nonlinear behavior of radiation intensity decay. Thus the resulting intercepts of the two curves
108 at AOD = 0 are quite different, 317 Wm⁻² with linear extrapolation and 349 Wm⁻² with nonlinear
109 regression, with a difference of 32 Wm⁻² when estimating ADRE. Also, for each F^{aer} we show the
110 corresponding AERONET F^0 (circles), based on the retrieved WVC and surface albedo, and calculated
111 with a radiative transfer model (e.g., Garcia et al., 2008; Derimian et al., 2008). We use the ADRE
112 obtained by averaging these F^0 (circles) values (bar at $F = 325$ Wm⁻² on the y-axis) as the benchmark
113 against which the extrapolation methods are evaluated.

114 Mathematically, our analysis can be summed up as a comparison between the extrapolated
115 ADRE

116
$$ADRE_{extrapol} = \frac{1}{n} \sum F_i^{aer} - F_{extrapol}^0 \quad (1)$$

117 and the AERONET ADRE

118
$$ADRE_{AERONET} = \frac{1}{n} \sum F_i^{aer} - \frac{1}{n} \sum F_i^0, \quad (2)$$

119 in where F_i^{aer} and F_i^0 is F^{aer} and F^0 , respectively, with i varying from one to the number of dataset, n .

120 Notably, the extrapolated F^0 ($F_{extrapol}^0$) derived with fits represents a single value for a dataset, but in the

121 AERONET, F^0 is determined side-by-side with each F^{aer} . $F_{extrapol}^0$ is calculated using fits as follows

122
$$F_i^{nonlin} = x_1 + x_2 * \exp(-x_3 * AOD_i); F_{extrapol}^{0,nonlin} = x_1 + x_2, \quad (3)$$

123
$$F_i^{lin} = x'_1 + x'_2 * AOD_i; F_{extrapol}^{0,lin} = x'_1, \quad (4)$$

124 in where F_i^{nonlin} and F_i^{lin} is estimated F^{aer} derived for each AOD with the nonlinear and linear method,

125 respectively. Constants of fits are x_1, x_2, x_3, x'_1 and x'_2 , and $F_i^{0,nonlin}$ and $F_i^{0,lin}$, thus $F_{extrapol}^0$ of the nonlinear

126 and linear fits, are provided with the constants.

127 Our decision to use the modeled F from AERONET, instead of pyranometer measurements, was

128 based on two different aspects. First, this allowed us to include a multiple number of sites, with very

129 different and varying aerosol conditions. Second, AERONET data provided interesting ancillary

130 measurements to support and better understand our analysis, WVC being the most crucial one. In

131 addition, the AERONET F s agree with pyranometer measurements with a correlation better than 99%

132 and the relative difference varies from 0.98 to 1.02 (Garcia et al., 2008). [Moreover, we tested the](#)

133 [analysis in two sites, Alta-Floresta and Goddard Space Flight Center \(GSFC\), by using pyranometer](#)

134 [measured fluxes \$F\$ and found no significant difference of the results in these two sites, if compared to](#)

135 [the corresponding analysis using the AERONET-modeled fluxes instead.](#)

136

137 3. Results

138 As further examples of determining ADRE using regression analysis, we show F^{aer} and AOD data from
139 four sites in Fig. 2. In addition, the linear (dashed line) and nonlinear decay (solid line) fits to the data
140 are shown. The bar on the vertical axis represents the average (with STD) value for F^0 . ~~Goddard Space~~
141 ~~Flight Center (GSFC)~~ (39° N, 77° W) (SZA = 70°) (Fig. 2a) and Rio-Branco (10° S, 68° W) (SZA =
142 70°) (Fig. 2b) represent cases in which the data are of sufficient quality for estimating ADRE: AOD
143 values reach close zero with only minor changes in WVC, aerosol optical properties and surface
144 reflectance for a given AOD, resulting in a narrow spread in the data. In these cases, since the nonlinear
145 decay represents a more realistic decay of radiation intensity (based on squared values of residuals), the
146 intersection of the nonlinear_fit with the AOD=0 axis (y-axis) is within the STD of the baseline value.
147 Dhadnah (26° N, 56° E) (SZA = 70°) (Fig. 2c) and GSFC at SZA = 22° (Fig. 2d) are examples of more
148 challenging cases: in Fig. 2c only data points with AOD > 0.2 exist so that a more extensive
149 extrapolation is needed, and in Fig. 2d there is significant scatter in the points.

150 Perhaps the most interesting feature shown in Fig. 2, which also significantly affects the quality
151 of ADRE estimation, is the correlation of F^0 with AOD. In Fig. 2a-d there is a negative correlation
152 while in 2b the correlation is positive. The negative correlation between F^0 and AOD is indirectly
153 caused mainly by a positive correlation of AOD with WVC due to humid airmasses with large aerosol
154 concentration. Only in some cases, where airmasses are dominated by dust aerosols, the correlation is
155 negative. With increasing AOD and WVC, the WVC dims an increasing fraction of the radiation
156 intensity – resulting in a smaller F^0 . The opposite occurs if AOD and WVC have a negative correlation.
157 Increase in the AOD as a function of WVC is presumably partly due to hygroscopic growth (e.g.,
158 Kitamori et al., 2009), although probably a major part of the correlation can be attributed to a large
159 variance in atmospheric conditions of aerosol properties and air humidity during seasons.

160 The intersections of the nonlinear decay fits (solid lines in Fig. 2) with the AOD = 0 axis –
161 313.5 W/m² (Fig. 2a), 295.9 W/m² (2b), 327.4 W/m² (2c) and 1008.9 W/m² (2d) – approximate the F^0
162 value at AOD = 0. This is clear from the figure, if one imagines straight line fits through the circles and
163 extrapolates fits down to AOD = 0. This approximation is, however, not necessarily a good one for the
164 mean F^0 , if F^0 and AOD correlate (through the AOD-WVC-correlation). For the negative correlation
165 cases (2a-d) the intersections of the nonlinear decay fits with the AOD = 0 axis tend to therefore over-
166 estimate the mean baseline F^0 (307.3 W/m² for 2a, 312.9 W/m² for 2c, and 972.1 W/m² for 2d) – as the
167 majority of F^0 values are below the extrapolated F^0 . Typically, for the positive correlation cases (2b,
168 mean of $F^0 = 303.4$ W/m²) the opposite occurs. As the linear fit obviously results in a lower estimation
169 of F^0 , the linear regression method can result often in a better estimation of the mean F^0 , as is clearly
170 the case in Fig. 2c (mean $F^0 = 306.7$ W/m²) and Fig. 2d (mean $F^0 = 973.0$ W/m²) – even if the nonlinear
171 regression is physically more correct.

172 The performance of the two different regression methods and, in particular, the WVC and AOD
173 correlation effect on the performance, is illustrated as scatter plots in Fig. 3. In Fig. 3a all data are
174 presented in ADRE (nonlinear decay method) and ADRE (AERONET $\Delta F^{average}$, Eq. 2) form. The colour
175 of the single points indicates the correlation of the WVC and AOD. In Fig. 3b the same is shown for the
176 linear regression case. Evidently a majority of the cases are such that WVC and AOD have a strong
177 positive correlation (red colored points). In addition, it seems that for most of these cases, the linear
178 regression method (Fig. 3b) results in a better ADRE estimation than the nonlinear decay regression
179 method (Fig. 3a). This means that the inaccuracy inherent in the linear regression cancels out errors
180 caused by the WVC and AOD correlation. For a weak WVC and AOD correlation, the nonlinear decay
181 method appears to be clearly better. ~~(Not shown, other parameters as surface albedo, ASYM or SSA~~
182 ~~do not play as a crucial role as WVC. We classified the ADRE estimates of the both methods against~~
183 ~~the baseline in respect of AOD, albedo, ASYM, SSA and WVC. It was evident that only WVC can~~

184 explain the observed differences of both methods when compared against the baseline. Moreover, we
185 confirmed, by modeling a short wavelength range (310 nm -500 nm), that this WVC-effect vanishes, if
186 some other wavelength band as e.g. the visible range of 400-700 nm containing no significant water
187 vapour absorption is under consideration, instead of the broadband wavelength range of F^{aer} .

188 Next we investigated possible geographical features of this correlation. Figure 4 shows the
189 WVC and AOD correlation (in the color scales) at all the sites available from AERONET~~included our~~
190 ~~study~~, in this case for ~~the~~ seasons: December-February (DJF, Fig. 4a), March-May (MAM, Fig. 4b),
191 June-August (JJA, Fig. 4c) and September-November (SON, Fig. 4d)~~season~~ (all years available). Most
192 of the points are colored either green or red, indicating an absent or a positive correlation. The strongest
193 positive correlation is for the stations in Europe and eastern USA, presumably due to aerosol
194 hygroscopic growth. This holds especially for the JJA and SON- seasons: The DJF and MAM- seasons
195 provide weaker positive correlation, indicating that the linear method can then provide there somewhat
196 underestimated ADRE. Interestingly, the strongest negative correlation appears during the JJA-season
197 in the west Sahara's region and Central-America, probably caused by a strong desert dust domination
198 and low WVC in the Saharan outflow region (Marsham et al., 2008). During those particular cases, the
199 linear method can significantly underestimate ADRE, as indicated by the points of largest negative
200 WVC vs. AOD correlation in Fig. 3b, while the nonlinear decay provides then a better estimate. The
201 blue points, representing a negative correlation (at least for this season) are all in the Saharan outflow
202 region (Marsham et al., 2008), with a strong desert dust domination and low WVC for larger AOD
203 eases.

204 Finally, the ADRE estimations of all data are grouped together in numerical form in Table 1. As
205 already evident from the figures, the nonlinear decay regression method overestimates (mean = -57.2
206 Wm^{-2}) while the linear method underestimates (mean = -39.4 Wm^{-2}) the magnitude of ADRE
207 (AERONET value = -46.1 Wm^{-2}). Overall, the linear method yields better results than the nonlinear

208 decay method.

209 Previous studies have shown that the AERONET WVC agrees well with radiosonde sounding
210 data (e.g., Prasad and Singh, 2009; Bokoye et al., 2007). We also compared AERONET WVC
211 measurements against radiosonde data from five sites (Alta-Floresta, Cuiaba-Miranda, Niamey,
212 Thessaloniki and Wallops) and observed similarly high correlations between these two data sources.
213 However, we wanted to assess in particular whether there exists any systematic dependence between
214 WVC from these two data sources as a function of AOD, which could affect our ADRE analysis based
215 on the modeled F . We found that while the ratio between the AERONET and radiosonde WVC is
216 essentially constant for AODs (at 500nm) larger than about 0.1, in many sites WVC can deviate for the
217 cases of smallest AOD (below 0.1). We estimated how our ADRE values (based on the F and AOD
218 relation) would change if we normalized the AERONET-modeled fluxes to incorporate the WVC from
219 the radiosonde measurements instead of AERONET-measured WVC. We found that the increased
220 WVC uncertainty at the lowest AOD values introduces an insignificant change in our ADRE estimates.

221

222 **4. Conclusions**

223 Determining the ADRE at the Earth's surface from radiative flux, F , measurements is not
224 straightforward because it involves the estimation of the flux without aerosols F^0 . This requires either
225 radiative transfer modelling or an extrapolation of F down to AOD = 0.

226 We have evaluated two such extrapolation methods: i) a linear fit and ii) an nonlinear decay fit
227 to the F and AOD data. As a reference we used the AERONET ADRE data in which F^0 (and F) is
228 calculated with radiative transfer modelling. Radiation attenuation due to multiple scattering and
229 absorption results typically in a near nonlinear decay of the intensity, and thus the nonlinear decay
230 regression is expected to give a better estimation of ADRE. This would be the case if the typically
231 positive correlation of WVC and AOD would not affect the dependency. F^0 represents an

232 unrealistically low WVC, resulting in an underestimation of attenuation caused by the WVC, and hence
233 a too large F^0 . This leads to an overestimation of the magnitude of ADRE. For stations and data series
234 in which there is no correlation between WVC and AOD, the nonlinear decay fit is superior.

235 As the WVC effect was found to be of such importance, we also investigated the geographical
236 correlation of WVC and AOD. The positive correlations clearly dominate, and clear negative
237 correlations occur predominantly in desert dust dominated data series, such as the regions at the
238 Saharan outflow. The strongest positive correlation was found in in stations in Europe and Eastern
239 USA. Our results indicate that the regression method, either linear or nonlinear, can readily produce a
240 significant error due to the correlation of WVC and AOD. Since for a majority of locations, AOD and
241 water vapour column (WVC) have a positive correlation, the linear method gives somewhat better
242 results in general than the nonlinear approach, for the reasons discussed above. However, there are
243 specific regions of strong negative WVC and AOD correlation, most notably in the Saharan dust
244 outflow region, where the opposite takes place and nonlinear approach results in better estimate for
245 ADRE. Therefore, based on our results we recommend that when the surface ADRE is estimated by
246 using pyranometer and AOD measurements, the site-specific correlation between WVC and AOD
247 should be also estimated to deduce whether linear or nonlinear approach is more suitable. We moreover
248 recommend to take a one step forward and additionally attempt to correct for the possible bias due to
249 WVC and AOD correlation. If the data for the WVC is available, then better ADRE accuracy is likely
250 achieved if the flux measurements are normalized to constant WVC amount with simple scaling
251 obtained from RT modeling.

252

253 **Acknowledgments.**

254 We thank the AERONET team, principal investigators and other participants for their effort in

255 establishing and maintaining the network. This study is supported by the Academy of Finland Doctoral
256 Programme ACCC and the Maj and Tor Nessling foundation. We also thank Larry Oolman from
257 Department of Atmospheric Science, University of Wyoming, for providing radiosonde- data of
258 atmospheric water vapour column abundance.

259

260 **References**

261 Bokoye, A. I., Royer, A., Cliche, P., and O'Neill, N.: Calibration of Sun Radiometer – based
262 atmospheric water vapor retrievals using GPS meteorology, *J. Atmos. Ocean. Tech.*, 24,
263 964–979, doi:10.1175/JTECH2011.1, 2007.

264 Bush, B. C. and Valero, F. P. J.: Spectral aerosol radiative forcing at the surface during the Indian
265 Ocean Experiment (INDOEX), *J. Geophys. Res.*, 107, 8003, doi:10.1029/2000JD000020,
266 2002.

267 Bush, B. C. and Valero, F. P. J.: Surface aerosol radiative forcing at Gosan during the ACE-Asia
268 campaign, *J. Geophys. Res.*, 108, 8660, doi:10.1029/2002JD003233, 2003.

269 Conant, W. C., Seinfeld, J. H., Wang, J., Carmichael, G. R., Tang, Y., Uno, I., Flatau, P. J.,
270 Markowicz, K. M., and Quinn, P. K.: A model for the radiative forcing during ACE-Asia derived
271 from CIRPAS Twin Otter and R/V Ronald H. Brown data and comparison with observations, *J.*
272 *Geophys. Res.*, 108, 8661, doi:10.1029/2002JD003260, 2003.

273 Derimian, Y., Léon, J.-F., Dubovik, O., Chiapello, I., Tanré, D., Sinyuk, A., Auriol, F., Podvin, T.,
274 Brogniez, G., and Holben, B. N.: Radiative properties of aerosol mixture observed during the
275 dry season 2006 over M'Bour, Senegal (African Monsoon Multidisciplinary Analysis campaign),
276 *J. Geophys. Res.*, 113, D00C09, doi:10.1029/2008JD009904, 2008.

277 Di Sarra, A., Pace, G., Meloni, D., De Silvestri, L., Piacentino, S., and Monteleone, F.: Surface
278 shortwave radiative forcing of different aerosol types in the central Mediterranean, *Geophys.*
279 *Res. Lett.*, 35, L02714, doi:10.1029/2007GL032395, 2008.

280 [Dubovik, O., and M. D. King, A flexible inversion algorithm for retrieval of aerosol optical properties](#)
281 [from Sun and sky radiance measurements, *J. Geophys. Res.*, 105\(D16\), 20673–20696,](#)
282 [doi:10.1029/2000JD900282, 2000.](#)

283

284 Dubovik, O., Smirnov, A., Holben, B. N., King, M. D., Kaufman, Y. J., Eck, T. F., and Slutsker, I.:
285 Accuracy assessments of aerosol optical properties retrieved from Aerosol Robotic Network
286 (AERONET) Sun and sky radiance measurements, *J. Geophys. Res.*, 105, 9791–9806,

287 doi:10.1029/2000JD900040, 2000.

288

289 Dumka, U. C., Satheesh, S. K., Pant, P., Hegde, P., and Krishna Moorthy, K.: Surface changes
290 in solar irradiance due to aerosols over central Himalayas, *Geophys. Res. Lett.*, 33, L20809,
291 doi:10.1029/2006GL027814, 2006.

292 [Eck, T. F., B. N. Holben, J. S. Reid, O. Dubovik, A. Smirnov, N. T. O'Neill, I. Slutsker, and S. Kinne,
293 *Wavelength dependence of the optical depth of biomass burning, urban, and desert dust aerosols, J.
294 *Geophys. Res.*, 104\(D24\), 31333–31349, doi:10.1029/1999JD900923, 1999.*](#)

295 García O. E., Díaz, A. M., Expósito, F. J., Díaz, J. P., Dubovik, O., Dubuisson, P., Roger, J.-
296 C., Eck, T. F., Sinuyk, A., Derimian, Y., Dutton, E. G., Schafer, J. S., Holben, B. N., and
297 García, C. A.: Validation of AERONET estimates of atmospheric solar surface fluxes and
298 aerosol radiative forcing by ground-based broadband measurements, *J. Geophys. Res.*, 113,
299 D21207, doi:10.1029/2008JD010211, 2008.

300 García O. E., Díaz, A. M., Expósito, F. J., Díaz, J. P., Redondas, A., and Sasaki, T.: Aerosol
301 radiative forcing and forcing efficiency in the UVB for regions affected by Saharan and Asian
302 Mineral Dust, *J. Atmos. Sci.*, 66, 1033–1040, doi:10.1175/2008JAS2816.1, 2009.

303 [García O.E., Díaz J.P., Expósito F.J., Díaz A.M., Dubovik O. and Derimian Y. Aerosol Radiative
304 Forcing: AERONET-Based Estimates, *Climate Models*, Dr. Leonard Druyan \(Ed.\), ISBN: 978-953-51-
305 0135-2, InTech, DOI: 10.5772/32287. Available from: \[http://www.intechopen.com/books/climate-
306 models/aerosol-radiative-forcing-aeronet-based-estimates\]\(http://www.intechopen.com/books/climate-models/aerosol-radiative-forcing-aeronet-based-estimates\), 275-296, 2012.](#)

307 Holben, B. N., Eck, T. F., Slutsker, I., Tanré, D., Buis, J. P., Setzer, A., Vermote, E., Reagan, J. A.,
308 Kaufman, Y. J., Nakajima, T., Lavenu, F., Jankowiak, I., and Smirnov, A.: AERONET – a Federated
309 Instrument Network and Data Archive for aerosol characterization, *Remote Sens.
310 Environ.*, 66, 1–16, doi:10.1016/S0034-4257(98)00031-5, 1998.

311 Intergovernmental Panel on Climate Change (IPCC): *Climate Change 2013: The Physical Science
312 Basis*, available at: <http://www.ipcc.ch/> (last access: January 2014), 2013.

313 Kaufman, Y. J., Tanré, D., Holben, B. N., Mattoo, S., Remer, L. A., Eck, T. F., Vaughan, J.,
314 Chatenet, B.: Aerosol radiative impact on spectral solar flux at the surface, derived
315 from principal-plane sky measurements, *J. Atmos. Sci.*, 59, 635–646, doi:10.1175/1520-
316 0469(2002)059<0635:AROSS>2.0.CO;2, 2002.

317 Kitamori, Y., Mochida, M., and Kawamura, K.: Assessment of the aerosol water content in urban
318 atmospheric particles by the hygroscopic growth measurements in Sapporo, Japan, *Atmos.
319 Environ.*, 43, 3416–3423, 2009.

320 Kudo, R., Uchiyama, A., Yamazaki, A., Sakami, T., and Kobayashi, E.: From solar radiation

321 measurements to optical properties: 1998–2008 trends in Japan, *Geophys. Res. Lett.*, 37,
 322 L04805, doi:10.1029/2009GL041794, 2010.

323 Loeb, N. G. and Su, W.: Direct aerosol radiative forcing uncertainty based on a radiative perturbation
 324 analysis, *J. Climate*, 23, 5288–5293, doi:10.1175/2010JCLI3543.1, 2010.

325 Markowicz, K. M., Flatau, P. J., Remiszewska, J., Witek, M., Reid, E. A., Reid, J. S., Bucholtz, A.,
 326 and Holden, B.: Observations and modeling of the surface aerosol radiative forcing during
 327 UAE2, *J. Atmos. Sci.*, 65, 2877–2891, doi:10.1175/2007JAS2555.1, 2008.

328 Marsham, J. H., Parker, D. J., Grams, C. M., Johnson, B. T., Grey, W. M. F., and Ross, A. N.:
 329 Observations of mesoscale and boundary-layer scale circulations affecting dust transport
 330 and uplift over the Sahara, *Atmos. Chem. Phys.*, 8, 6979–6993, doi:10.5194/acp-8-6979-
 331 2008, 2008.

332

333 Myhre, G.: Consistency between satellite-derived and modeled estimates of the direct aerosol
 334 effect, *Science*, 325, 187, doi:10.1126/science.1174461, 2009.

335 Prasad, A. K. and Singh, R. P.: Validation of MODIS Terra, AIRS, NCEP/DOE AMIP-II
 336 Reanalysis-2, and AERONET Sun photometer derived integrated precipitable water vapor
 337 using ground-based GPS receivers over India, *J. Geophys. Res.*, 114, D05107,
 338 doi:10.1029/2008JD011230, 2009.

339 Roger, J. C., Mallet, M., Dubuisson, P., Cachier, H., Vermote, E., Dubovik, O., and De15
 340 spiau, S.: A synergetic approach for estimating the local direct aerosol forcing: application
 341 to an urban zone during the Exprience sur Site pour Contraindre les Modèles de Pollution
 342 et de Transport d’Emission (ESCOMPTE) experiment, *J. Geophys. Res.*, 111, D13208,
 343 doi:10.1029/2005JD006361, 2006.

344 Satheesh, S. K. and Ramanathan, V.: Large differences in tropical aerosol forcing at the top of
 345 the atmosphere and Earths surface, *Nature*, 405, 60–63, doi:10.1038/35011039, 2000.

346 Satheesh, S. K., Vinoj, V., and Krishna Moorthy, K.: Radiative effects of aerosols at an urban
 347 location in southern India: Observations vs. model, *Atmos. Environ.*, 44, 5295–5304,
 348 | doi:10.1016/j.atmosenv.2010.07.020, 2010.

349

350 Table 1. The estimated ADRE(F^{ver}) with standard deviations compared with the AERONET value.

351 MAD = Mean Absolute Deviation. Units are in Wm^{-2} , except for the correlation coefficient (CC).

Parameter	AERONET	Method	Estimate	Est. - AERONET	CC	MAD
ADRE	-46.1 ± 20.4	Exp. decay	-57.2 ± 23.4	-11.1	0.75	13.4
		Linear	-39.4 ± 16.9	+6.7	0.89	8.9

352

353

354

355

356

357

358

359

360

361

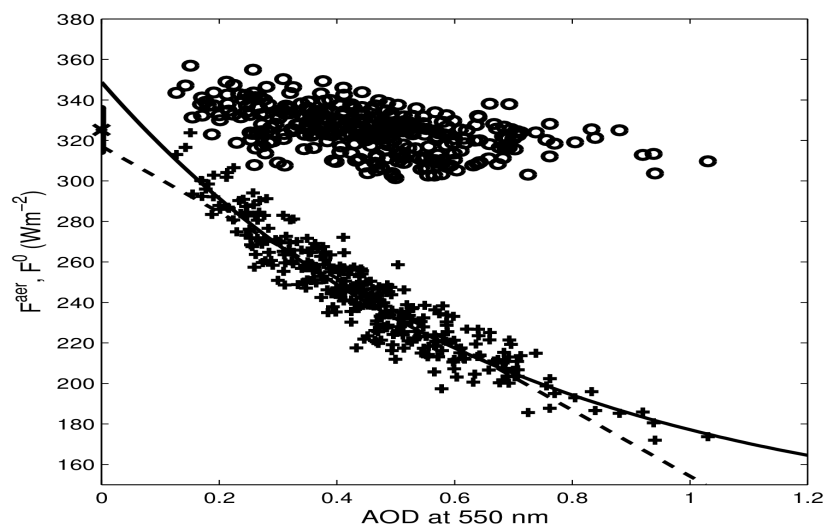
362

363

364

365

366



367 Figure 1: Radiative flux with aerosols F^{aer} (plusses) and without aerosols F^0 (circles) as a function of

368 AOD for the AERONETsite in Kanpur in March-May and with $SZA = 69^\circ \pm 1.5^\circ$. The bar on the

369 vertical axis represents the mean value of the estimated F^0 (all circles). The solid and dashed lines

370 represent the exponential and linear fits to the data, respectively.

371

372

373

374

375

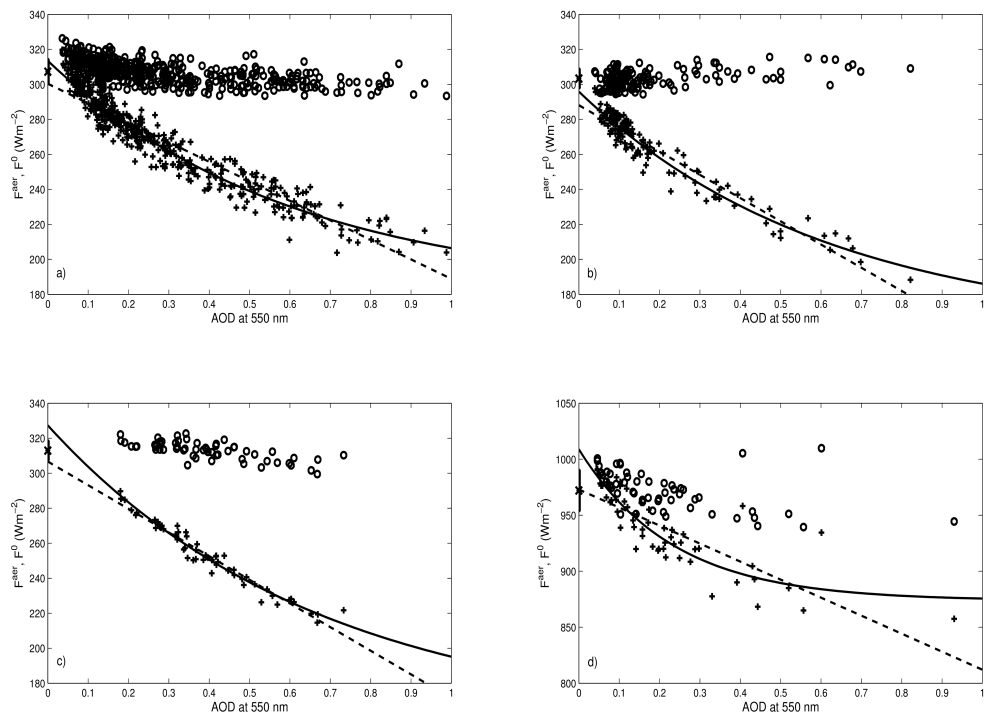
376

377

378

379

380



381 Figure 2: Same as Fig. 1, but for the June-August season in a) GSFC (SZA=70°), b) Rio-Branco (SZA
382 = 70°), c) Dhadnah (SZA = 70°), d) GSFC (SZA = 22°).

383

384

385

386

387

388

389
390
391
392
393
394
395
396
397
398
399
400
401
402
403
404
405
406
407
408
409
410
411
412
413
414
415
416
417
418
419
420
421
422
423
424
425
426
427
428
429
430
431
432
433
434

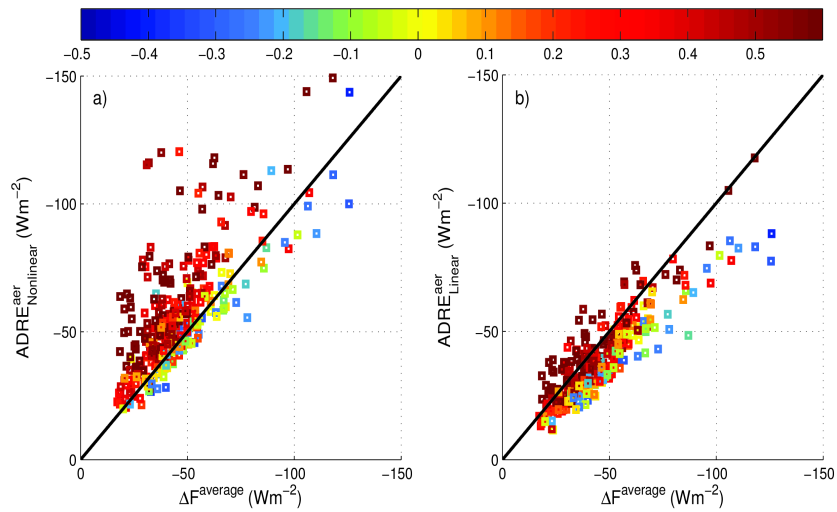
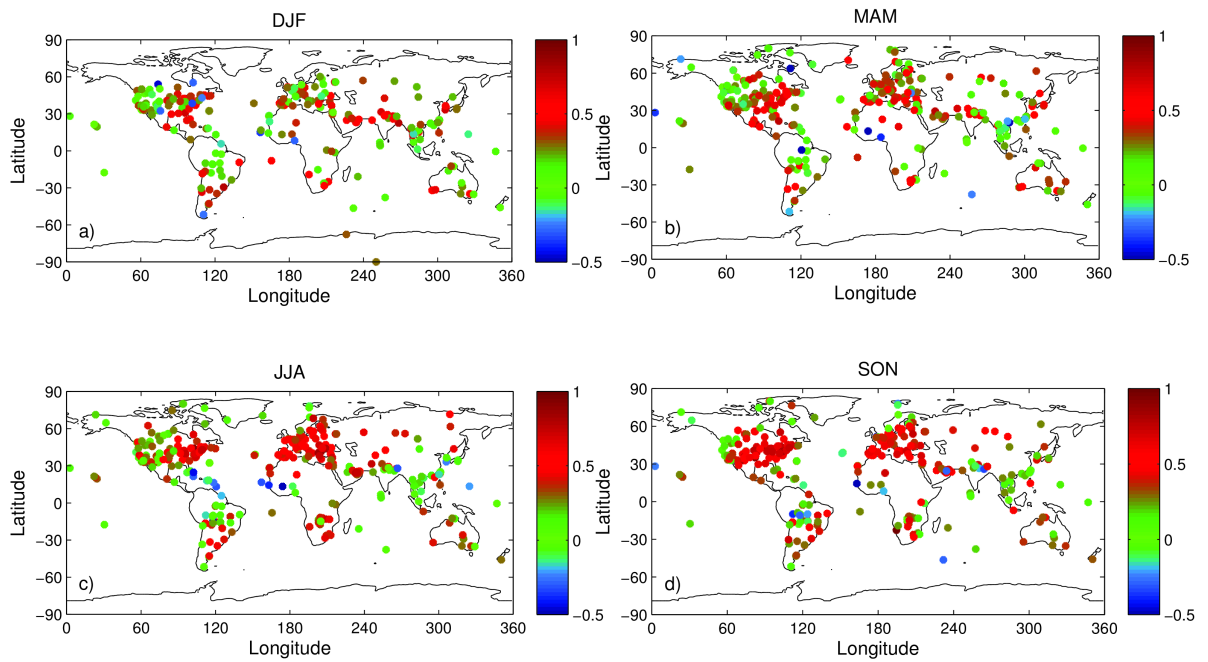


Figure 3: ADRE predicted with exponential decay (a) and linear (b) regression methods (equation 1), compared with AERONET values (equation 2). The color of the data points represents the correlation coefficient of the AOD and WVC correlation, with red color indicating positive and blue color negative correlation.



436
 437
 438
 439
 440
 441
 442
 443
 444
 445
 446
 447

Figure 4: Geographical distribution of the AOD and WVC correlation, at all AERONET stations considered in this study for [a\) December-February](#), [b\) March-May](#), [c\) June-August](#) and [d\) September-November](#) (all available years).